Nanoscale

RSC Publishing

COMMUNICATION

View Article Online
View Journal | View Issue

Cite this: *Nanoscale*, 2013, **5**, 9517

Received 5th June 2013
Accepted 29th July 2013

DOI: 10.1039/c3nr02912c

www.rsc.org/nanoscale

Nanophasic biodegradation enhances the durability and biocompatibility of magnesium alloys for the next-generation vascular stents

Lin Mao,†[abc] Li Shen,†[d] Jialin Niu,[b] Jian Zhang,[b] Wenjiang Ding,[bc] Yu Wu,[a] Rong Fan*[ae] and Guangyin Yuan*[bc]

Biodegradable metal alloys emerge as a new class of biomaterials for tissue engineering and medical devices such as cardiovascular stents. Deploying biodegradable materials to fabricate stents not only obviates a second surgical intervention for implant removal but also circumvents the long-term foreign body effect of permanent implants. However, these materials for stents suffer from an uncontrolled degradation rate, acute toxic responses, and rapid structural failure presumably due to a non-uniform, fast corrosion process. Here we report that highly uniform, nanophasic degradation is achieved in a new Mg alloy with unique interstitial alloying composition as the nominal formula Mg–2.5Nd–0.2Zn–0.4Zr (wt%, hereafter, denoted as JDBM). This material exhibits highly homogeneous nanophasic biodegradation patterns as compared to other biodegradable metal alloy materials. Consequently it has significantly reduced degradation rate determined by electrochemical characterization. The *in vitro* cytotoxicity test using human vascular endothelial cells indicates excellent biocompatibility and potentially minimal toxic effect on arterial vessel walls. Finally, we fabricated a cardiovascular stent using JDBM and performed *in vivo* long-term assessment *via* implantation of this stent in an animal model. The results confirmed the reduced degradation rate *in vivo*, excellent tissue compatibility and long-term structural and mechanical durability. Thus, this new Mg-alloy with highly uniform nanophasic biodegradation represents a major breakthrough in the field and a promising material for manufacturing the next generation biodegradable vascular stents.

Atherosclerosis, a chronic pathological process, is the leading mechanism of cardiovascular disease (CVD), which remains the number one cause of death globally. Implantation of a vascular stent is the mainstay of surgical treatment to rescue the function of diseased coronary arteries. In the past decades, a variety of materials, including stainless steel,[1] nickel–titanium alloys,[2] tantalum and nitinol,[3] have been used to manufacture vascular stents. Recently, a new class of vascular stents made of biodegradable Mg alloys has been reported to show unique advantages compared to the conventional stents.[4] It was used as a short-term structural support and allows for full recovery of arteries without leaving behind foreign materials.[4] Mg alloys can dissolve completely in the physiological environment and the degradation products can be metabolized and absorbed by the body and thus obviate a second surgical intervention for implant removal, which is currently a standard procedure, and thus minimize the physical irritation and chronic inflammatory response.[2] The unique properties of Mg alloys offer the possibility of enhanced wound healing and reconstruction of vascular compliance during tissue recovery.[5]

However, the Mg alloys being employed for vascular stents typically have low corrosion resistance under physiological conditions associated with a highly inhomogeneous degradation morphology, rapid release of degradation products and early loosening or disintegration of the implants, causing complete failure of the device before the time required for the tissue to become fully healed. The inhomogeneous degradation leads to local stress concentration and decrease of mechanical strength, consequently subjecting the Mg-alloy stent to unexpected fracture way before the anticipated lifetime by design. Therefore, it is highly desired to have a new material for vascular stents that remains biodegradable but with new properties that can address all these challenges *via* significantly increasing the degradation uniformity, reducing the corrosion rate, and improving the synchronization between the implant biodegradation and the tissue recovery.

[a]*Department of Biomedical Engineering, Yale University, New Haven, CT 06511, USA. E-mail: rong.fan@yale.edu*

[b]*National Engineering Research Center of Light Alloy Net Forming, Shanghai Jiao Tong University, Shanghai 200240, China. E-mail: gyyuan@sjtu.edu.cn*

[c]*State Key Laboratory of Metal Matrix Composite, Shanghai Jiao Tong University, Shanghai 200240, China*

[d]*Shanghai Institute of Cardiovascular Diseases, Department of Cardiology, Zhongshan Hospital, Fudan University, Shanghai 200032, China*

[e]*Yale Comprehensive Cancer Center, New Haven, CT 06520, USA*

† L. Mao and L. Shen contributed equally to this work.

Here we report on a highly homogeneous nanophasic degradation mechanism observed in a new Mg alloy Mg–2.5Nd–0.2Zn–0.4Zr (wt%, JDBM), which resulted in significantly improved corrosion uniformity and markedly reduced corrosion rate. This material shows minimal vascular toxicity and excellent biocompatibility *via in vitro* evaluation with human vascular endothelial cells. Finally, vascular stent devices were manufactured from JDBM and implanted into a rabbit for long-term *in vivo* evaluation. The results confirm excellent biocompatibility and long-term structural and mechanical durability, suggesting the great promise of this new material to address the aforementioned challenges. It represents a breakthrough in biodegradable alloy materials for the next generation vascular stent applications.

Results and discussion

Chemical structure and micromorphological analysis of degraded surfaces

The chemical composition of JDBM is shown in Table 1. Two other conventional biodegradable alloys (WE43 and AZ31) are also listed in this table and used in this study for comparison.

We carried out the first controlled degradation experiment *in vitro* by immersing the polished surfaces of these materials in artificial plasma (6.8 g L^{-1} NaCl, 0.2 g L^{-1} $CaCl_2$, 0.4 g L^{-1} KCl, 0.1 g L^{-1} $MgSO_4$, 2.2 g L^{-1} $NaHCO_3$, 0.126 g L^{-1} Na_2HPO_4 and 0.026 g L^{-1} NaH_2PO_4) and the degradation morphology was examined by Field Emission Scanning Electron Microscopy (FESEM) as shown in Fig. 1. JDBM exhibits a very uniform and smooth corrosion surface. The corrosion pits are homogeneous with nanophasic degradation patterns over a large scale, which has not been observed in other materials at this level of uniformity. In contrast, large pits of local degradation (pitting corrosion) are extensively observed on WE43 and AZ31 substrates (Fig. 1c and e). While the surface of WE43 exhibits a mixed degradation mechanism, the macroscopic large pits would eventually determine the durability and biocompatibility of the materials for implantation. The degradation mechanism of Mg alloys in a chloride containing biofluid is governed by the micro-galvanic corrosion and readily subjected to severe pitting corrosion due to the nonuniform distribution of second alloy phases and nonequilibrium grain boundaries. In order to reduce the degradation rate, it is critical to control the microscopic corrosion pattern and suppress the pitting corrosion.

Electrochemical characterization and the degradation mechanism

As the cyclic polarization measurement can distinguish different corrosion processes and quantify their contribution to the total rate of degradation, we performed such an analysis to further compare JDBM and two other Mg alloys with regard to their susceptibility to pitting corrosion in artificial plasma (Fig. 2a). In a cyclic polarization curve, the forward scan represents the polarization behavior of the non-corroded areas while the reverse scan is associated with the corroded areas. Generally, the area with a more negative potential in Mg alloys is corroded and the area with a more positive potential is protected. For the JDBM alloy, the corrosion potential of the reverse scan is greater than that of the forward scan ($E+ < E-$), which means the corrosion of the corroded area on JDBM that acts as the cathode is likely to be suppressed by the non-corroded area, while the non-corroded area that acts as the anode is prone to be eroded. As a result, JDBM experiences a homogeneous corrosion due to the anode and cathode switch in the galvanic corrosion. For WE43 and AZ31 alloys, however, the shift behavior from the forward scan to the reverse scan appears to be the opposite ($E+ > E-$). Consequently, the corrosion of corroded areas on WE43 and AZ31 substrates acting as the anode is accelerated by the non-corroded areas that act as the cathode and hence the two alloys suffer from severe local pitting corrosion. This result is in good agreement with the morphological examination of the degraded surfaces of JDBM, WE43 and AZ31 in artificial plasma (Fig. 1) from an electrochemical viewpoint. The *in vitro* corrosion rate of JDBM is 0.337 mm per year while those of WE43 and AZ31 alloys are 0.681 and 0.412 mm per year, respectively (Fig. 2b). The observation that this new Mg-alloy material has reduced corrosion rate and homogeneous degradation pattern can be attributed to several factors. It is well known that micro- and nano-structural refinement of Mg alloys can lead to significant improvement in the degradation response due to the alteration of passive layer characteristics.[6] Rare earth (RE) addition to Mg in general improves the anti-corrosion response by inhibiting Mg^{2+} cation release through the MgO layer in Mg alloys[7] and forming a rare-earth oxide film to passivate further corrosion in an aqueous environment.[8,9] A conventional alloying element zirconium (Zr) is a well-known grain refiner and it can reduce the detrimental influence of iron on the corrosion resistance by combining it with iron as insoluble particles.[10] Furthermore, the main constituent phases of JDBM are α-Mg and $Mg_{12}Nd$, and the corrosion potential of $Mg_{12}Nd$ is only slightly more positive than that of α-Mg, which is believed to slow down the galvanic corrosion and also leads to highly uniform, localized degradation at the nanometer scale.[11] Furthermore, the absolute potential difference ($|E+ - E-|$) of JDBM (0.06 V) is smaller than those of WE43 and AZ31 alloys (0.19 V and 0.14 V, respectively) in the cyclic polarization measurements, indicating a lower corrosion rate on the JDBM substrate due to the decrease of potential difference between the galvanic couples. The increase in repassivation tendencies of rare earth elements and small potential difference between the second phase particles and α-Mg achieved in this material together resulted in an enhanced resistance to corrosion under physiological conditions and potentially long-term durability. Thus, the results of the cyclic polarization measurements are in accordance with the morphological examination that shows the uniform nanophasic degradation surface of our new materials.

Table 1 Chemical compositions (wt%) of JDBM, WE43 and AZ31 alloys

Alloy	Nd	Zr	Al	Zn	Y	Gd	Mn	Mg
JDBM	2.50	0.44	—	0.21	—	—	—	Bal.
WE43	2.19	0.51	—	—	3.94	0.92	—	Bal.
AZ31	—	—	2.89	0.92	—	—	0.25	Bal.

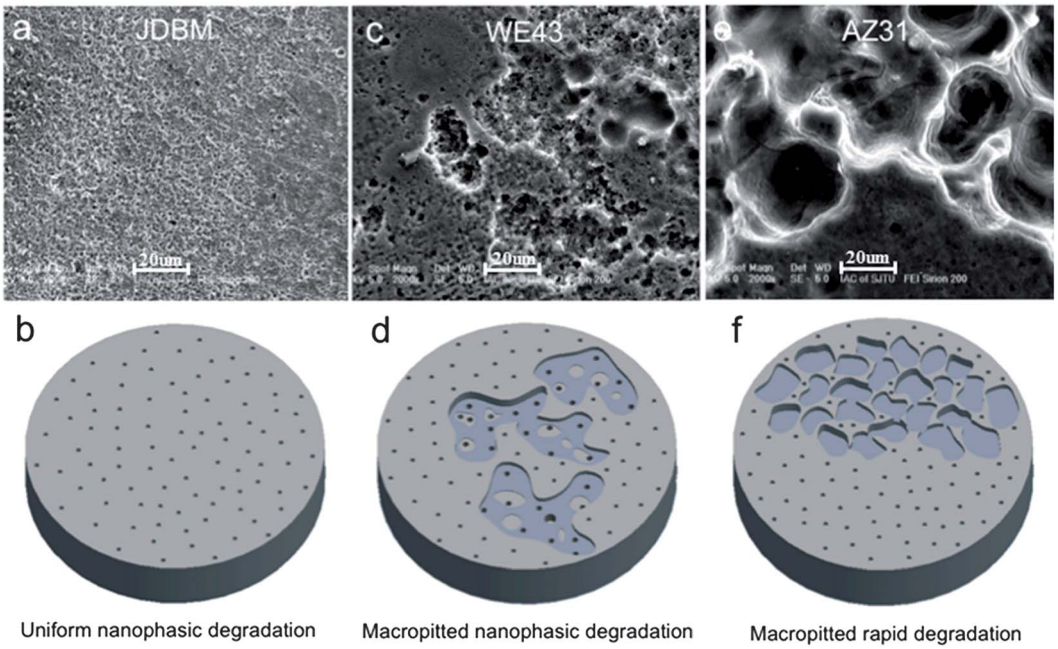

Fig. 1 Surface morphology and the schematic diagram of the corresponding degradation mechanism of JDBM (a and b), WE43 (c and d) and AZ31 (e and f) alloys. The surface of the new Mg-alloy (JDBM) upon exposure to artificial plasma displays a highly uniform array of nanopits with typical size less than 500 nm. In contrast, both WE43 and AZ31 alloys show macroscopic pitting or delamination that dominates the degradation process and results in a fast degradation rate and ultimately structural failure.

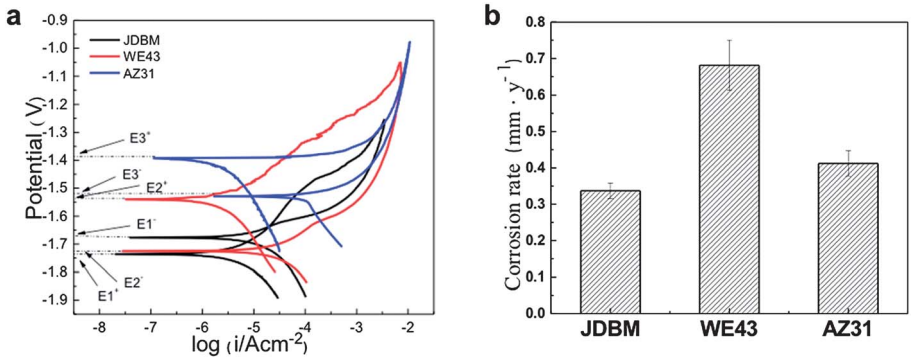

Fig. 2 Electrochemical characterization of the Mg-alloy degradation processes. (a) Cyclic polarization curves of JDBM, WE43 and AZ31 alloys tested in artificial plasma and (b) degradation rates of JDBM, WE43 and AZ31 alloys after 10 days of immersion in artificial plasma.

Vascular cytotoxicity and biocompatibility test *in vitro*

To further evaluate the vascular biocompatibility and cytotoxicity of this material compared with two conventional biodegradable metal alloys used for stents, we performed an *in vitro* test with human umbilical vein endothelial cells (HUVECs). First, we examined the response of HUVACs in the presence of different Mg alloy extracts. The results for different extract dilutions show a slight negative effect on HUVECs' viability (grade 1) in the first day incubation, but ramp up back to normal growth and cell viability in all tests with different extracts on days 3 and 5, reflecting a minimal cytotoxicity and rapid restoration of normal cell behavior (Fig. 3a). According to ISO 10993-5: 1999,[12] all three alloys meet the criteria of *in vitro* biosafety suitable for surgical applications. The apoptosis and necrosis ratios of HUVECs in different Mg extracts were measured with flow cytometry. Both ratios for HUVECs treated with the JDBM extract are lower than those for the cells treated with WE43 and AZ31 extracts (Fig. 3b1–b3). We also performed morphological characterization with HUVECs cultured in different Mg alloy extracts for a period of 24 h. HUVECs appear normal and healthy with the morphology of flattened spindles (Fig. 3c1–c4). Statistic analysis shows that there is no significant difference ($P > 0.05$) in the cell morphology, cell area and aspect ratio amongst the HUVEC samples treated with the Mg alloy extracts and with the negative control (Fig. 3d). The proliferation of HUVECs through 24 h incubation was determined by 5-bromo-20-deoxy-uridine (BrdU) incorporation, and the proliferation potential of HUVECs cultured in the JDBM extract is comparable to that in the negative control (90.24 ± 9.66) and

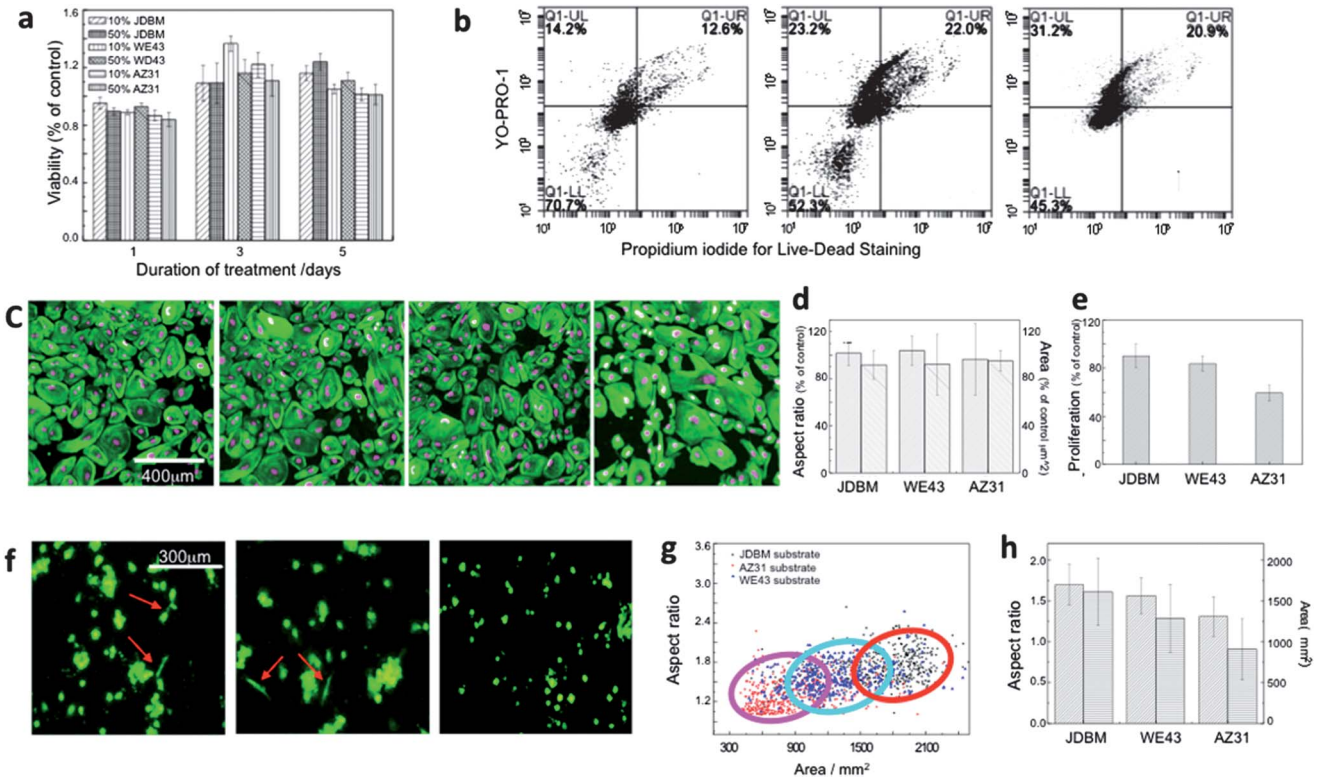

Fig. 3 Cytotoxicity and cytocompatibility tests *in vitro* on human endothelial cells. (a) HUVEC viability shown as the percentage of viable cells in the control after 1, 3 and 5 days of culture in the media containing JDBM, WE43 and AZ31 extracts (10% and 50%), respectively. (b) The ratio of apoptotic or necrotic cells is analyzed by flow cytometry on HUVECs treated with JDBM, WE43 and AZ31 extracts (from left to right). (c) Immunofluorescence images showing the morphology of HUVACs in the negative control and treated with JDBM, WE43 and AZ31 (from left to right) extracts for 24 h. The cells were fixed and stained for cytoskeleton (phalloidin: green) and nuclei (DRAQ5: magenta). (d) Cell area and aspect ratio of HUVECs cultured in JDBM, WE43 and AZ31 extracts for 24 h as compared to the negative control. (e) Proliferation ratio of HUVECs cultured in JDBM, WE43 and AZ31 extracts for 24 h as compared to the negative control. (f) Live cell observation of cell attachment and elongation. HUVECs were seeded directly on JDBM, WE43 and AZ31 metal substrates (from left to right) and cultured for 24 h. Cells were prestained with the live cell tracker dye. Statistical analysis of all the cells in terms of (g) single-cell scatter plot and (h) mean cell area and aspect ratio of all the HUVECs seeded and grown on the surface of JDBM, WE43 and AZ31 substrates, respectively.

higher than those in WE43 (83.74 ± 6.19) and AZ31 (59.35 ± 6.51) extracts (Fig. 3e). The result indicates that the JDBM alloy extract has a minimal adverse effect on primary human endothelial cells.

The physiological response of endothelial cells adjacent to an Mg alloy stent is believed to be strongly affected by the release of ions from the degrading metal surface. The selected alloying elements and chemical composition should be hemocompatible and not cause local or systemic toxicity. Of all conventional alloying elements, aluminum (Al) is usually added to Mg to improve the strength and corrosion resistance in industrial structural materials. However, Al has adverse effects *in vivo* and the tolerable mass content is far below that of other metal elements in Mg alloys.[13–15] Thus, Al is unfavorable to be applied to Mg alloys for implant applications. Meanwhile, it is reported that severe hepatotoxicity has been detected after the administration of cerium, praseodymium and yttrium[16] and Mg alloys with additives of manganese and yttrium may have negative effects on the cell viability.[17] As mentioned above, rare-earth addition can significantly enhance the corrosion resistance of Mg alloys in a chloride containing environment. Based on these design considerations, we chose a light RE element neodymium (Nd), accompanied by the nutrient element Zn and the grain refiner Zr as the alloying elements to develop a novel Mg alloy Mg–2.5Nd–0.2Zn–0.4Zr (wt%, JDBM). The alloying content in JDBM is only half of that in WE43 and without any heavy rare-earth elements. Hence, we can maintain the biosafety of JDBM as an implant material from the biomaterial design point of view.

To evaluate the response of endothelial cells to the stent materials, HUVEC suspension was seeded directly onto the JDBM, WE43 and AZ31 substrates, respectively (Fig. 3f). We observed distinguishable differences among these materials. A fraction of HUVECs exhibit the morphology similar to those cultured under normal conditions in a Petri dish. We observed pseudopodial spreading on JDBM and WE43 substrates, as shown by the arrow points. However, HUVECs on the AZ31 substrate appeared to be rounded with inefficient cell spreading, indicating that the AZ31 substrate does not allow HUVECs to attach well and spread. Quantitative analyses of the cell surface area and aspect ratio of HUVECs grown on the three substrates were performed by a high-content image analysis program (cell prolifer 2.0, the Broad Institute of MIT) (Fig. 3g and h).[18] We observed that both the cell area and aspect ratio

decrease when cultured on JDBM compared with the cells cultured on WE43 and AZ31. It is apparent that the JDBM substrate offers a more favorable surface for adhesion and spreading of HUVECs. This improvement is presumably attributed to the relatively slow, homogeneous nanophasic degradation. In contrast, the impaired cell adhesion and growth on AZ31 is due, in part, to the high corrosion rate and proton accumulation in the vicinity of a corroding surface, which are undesirable for cell functioning and can cause high cell osmolarity.[19–21] The chemical and topographical properties of implants are increasingly recognized as important cues that influence the response of vascular cells *in vivo* as well as *in vitro* in terms of cell adhesion, spreading, migration, differentiation and mechanotransduction signaling.[22] The morphology of cells can be altered indirectly by the topographical cues through orienting or organizing the cytoskeleton and polarizing cells with different functional behavior.

Evaluation of the long-term durability and efficacy *in vivo*

Finally we machined a vascular stent using the new Mg alloy material JDBM and conducted *in vivo* evaluation for its long-term durability and biocompatibility. The stent was fabricated with the classical hollow mesh pattern and implanted in a rabbit abdominal aorta for up to 16 weeks. We assessed the mechanical properties of the stent *in vivo* including expansion and recoiling. We also examined the long-term intimal hyperplasia in the vicinity of the stent. The JDBM stent deployed within the abdominal aorta was monitored by the intravascular ultrasound (IVUS) imaging as shown in Fig. 4. We found that the JDBM stent was completely expanded and well apposed to the vessel wall, with no sign of early recoil or fracture (Fig. 4a and c). At 16 weeks after stenting, the follow-up angiography and IVUS images demonstrated no obvious occlusion and neointimal formation in the stent (Fig. 4b and d). This result is highly promising and the major improvement in the mechanical durability and biocompatibility can be reasonably attributed to the reduced and highly uniform nanophasic degradation mechanism, which makes JDBM an ideal candidate for the next-generation biodegradable stent application.

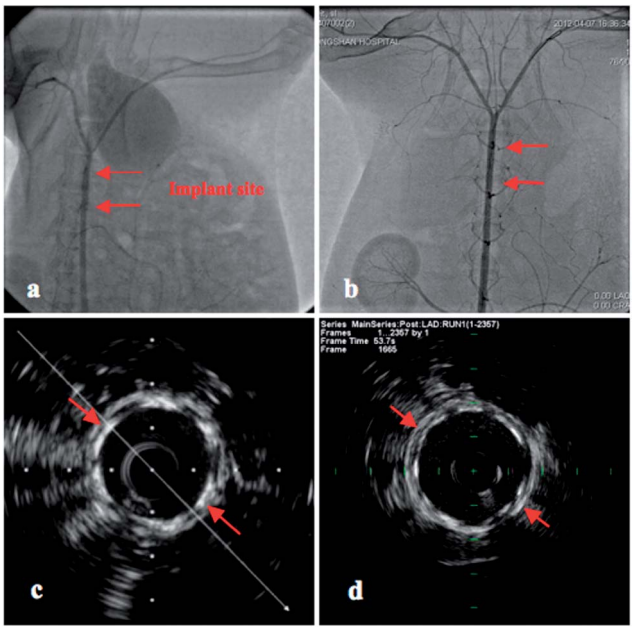

Fig. 4 The as-implanted (a and c) and 16-week follow-up (b and d) angiographic and the corresponding longitudinal reconstruction IVUS images of the abdominal aorta after JDBM stent implantation. Note the increased plaque volume and vessel size (arrow heads) at 16 weeks with the nearly complete absence of neointimal hyperplasia.

In conclusion, we have demonstrated that the new Mg-alloy material, JDBM, exhibits a unique biodegradation mechanism characterized by a highly uniform, nanophasic degradation pattern and consequently reduced degradation rate. Such a mechanism could contribute to both improved cytocompatibility and material durability. A systematic study on the *in vitro* biocompatibility test of JDBM in comparison with two conventional degradable metal alloys used for vascular stents shows that JDBM has a minimal negative effect on the HUVEC viability, growth and proliferation and the JDBM substrate offers a much more favorable surface for endothelial cell adhesion and spreading. Furthermore, a vascular stent was fabricated using the JDBM alloy and implanted in a rabbit model for long-term *in vivo* evaluation. The result suggests that the JDBM alloy stent has significantly improved mechanical durability and long-term biocompatibility with no sign of the development of occlusion and neointimal formation in the stent-supported vessel. Therefore, this new material showing a nanophasic degradation mechanism exhibits significantly enhanced performance both mechanically and physiologically, and thus is a promising material for future biodegradable vascular stent applications.

Materials and methods

Material preparation

The ingots of JDBM, WE43 and AZ31 alloys were prepared solution treatment (T4), extruded and annealed. The specimens (Ø 12 × 5 mm) were ground, polished and cleaned.

Degradation test *in vitro* and electrochemical characterization

The immersion test was performed according to ASTMG31-72 (ref. 23) in artificial plasma for 240 h at 37 °C and buffered at pH = 7.4. The corroded samples were cleaned with a chromic acid solution for removing the corrosion products, then the mean corrosion rates were calculated and the corroded surfaces were observed using FE-SEM. Cyclic polarization measurement was carried out using an Advanced Electrochemical System PARSTAT 2273 with a polarization scan at a rate of 1 mV s^{-1}.

Cytotoxicity test and vascular cell test *in vitro*

The cytotoxicity test was carried out by indirect contact using a standard MTT method.[17] The extract was prepared using EBM (Lonza, Cat. # CC-3156) serum free medium with the surface area of extract medium ratio of 1.25 cm^2 mL^{-1}. HUVECs were stained with phalloidin (Life Technologies-Invitrogen, Cat. # A22282) and DRAQ5 (Cell Signaling Technology, Cat. # 4084S) to identify the cell morphology and also stained with YO-PRO-1

(Life Technologies-Invitrogen, Cat. # Y3603) and propidium iodide (PI, SIGMA-ALDRICH, Cat. # P4170) to assess the apoptosis and necrosis ratios with a flow cytometer. Proliferating HUVECs were monitored by BrdU incorporation into nuclei of dividing cells for 30 min, followed by BrdU mouse mAb labelling and anti-mouse IgG (H + L) detection (Cell Signaling Technology, Cat. # 6813). HUVECs were seeded onto JDBM, WE43 and AZ31 substrates at a cell density of 2×10^5 cell mL^{-1} for 24 h, then rinsed and the remaining cells were stained by Cell Tracker (Invitrogen blue dye, Cat. # C7025) to investigate the direct cell response to various Mg alloy substrates.

Manufacturing of the JDBM vascular stent and the test for long-term durability *in vivo*

A JDBM stent with original dimensions of Ø 3 × 14 mm was fabricated by our group. Animal experiments were conducted under an Ethic Committee approved protocol in accordance with the Animal Welfare Act and the NIH Guide for Care and Use of Laboratory Animals. Serial angiography and IVUS imaging were performed after intracoronary administration of 0.2 mg nitroglycerin immediately after the procedure and at follow-up.

Author contributions

L. M. and G. Y. Y. conceived the project and designed experiments for material synthesis and structural characterization. L. M. and R. F. designed the *in vitro* cell assays. L. M. and Y. W. performed *in vitro* cell assay experiments and analyzed data. L. M. and L. S. performed the material characterization, relevant data collection and data analysis. All the authors contributed to the writing of the manuscript.

Notes

The authors declare no competing financial interest.

Acknowledgements

This work was supported by the National Nature Science Foundation of China (no. 51174136), National Basic Research Program ("973" Program) of China (2011CB503905), Science and Technology Commission of Shanghai Municipality (no. 11DJ1400301) and the National Key Technology R&D Program of China (2012BAI18B01). Research at Yale University was supported by the new faculty startup fund (PI: R.F.).

References

1 S. Windecker, R. Simon, M. Lins, V. Klauss, F. R. Eberli, M. Roffi, G. Pedrazzini, T. Moccetti, P. Wenaweser and M. Togni, *Circulation*, 2005, **111**, 2617–2622.
2 D. Wever, A. Veldhuizen, J. De Vries, H. Busscher, D. Uges and J. Van Horn, *Biomaterials*, 1998, **19**, 761–769.
3 B. O'Brien, W. Carroll and M. Kelly, *Biomaterials*, 2002, **23**, 1739–1748.
4 B. Zberg, P. J. Uggowitzer and J. F. Löffler, *Nat. Mater.*, 2009, **8**, 887–891.
5 L. Xu, G. Yu, E. Zhang, F. Pan and K. Yang, *J. Biomed. Mater. Res., Part A*, 2007, **83**, 703–711.
6 K. Ralston and N. Birbilis, *Corrosion*, 2010, **66**, 75005.
7 F. Zucchi, V. Grassi, A. Frignani, C. Monticelli and G. Trabanelli, *J. Appl. Electrochem.*, 2006, **36**, 195–204.
8 S. Krishnamurthy, M. Khobaib, E. Robertson and F. Froes, *Mater. Sci. Eng.*, 1988, **99**, 507–511.
9 H. Yao, Y. Li and A. Wee, *Electrochim. Acta*, 2003, **48**, 4197–4204.
10 E. F. Emley, *Principles of magnesium technology*, 1966.
11 J. W. Chang, Ph.D dissertation, Shanghai Jiao Tong University, 2008.
12 ISO 10993-5, *Biological evaluation of medical devices. Tests for in vitro cytotoxicity*, 1999.
13 C. Yuen and W. Ip, *Acta Biomater.*, 2010, **6**, 1808–1812.
14 M. T. Colomina, J. L. Esparza, J. Corbella and J. L. Domingo, *Neurotoxicol. Teratol.*, 1998, **20**, 651–656.
15 S. S. A. El-Rahman, *Pharmacol. Res.*, 2003, **47**, 189–194.
16 Y. Nakamura, Y. Tsumura, Y. Tonogai, T. Shibata and Y. Ito, *Toxicol. Sci.*, 1997, **37**, 106–116.
17 X. Gu, Y. Zheng, Y. Cheng, S. Zhong and T. Xi, *Biomaterials*, 2009, **30**, 484–498.
18 L. Kamentsky, T. R. Jones, A. Fraser, M. A. Bray, D. J. Logan, K. L. Madden, V. Ljosa, C. Rueden, K. W. Eliceiri and A. E. Carpenter, *Bioinformatics*, 2011, **27**, 1179–1180.
19 G. Song, *Corros. Sci.*, 2007, **49**, 1696–1701.
20 G. Song and S. Song, *Adv. Eng. Mater.*, 2007, **9**, 298–302.
21 F. Witte, N. Hort, C. Vogt, S. Cohen, K. U. Kainer, R. Willumeit and F. Feyerabend, *Curr. Opin. Solid State Mater. Sci.*, 2008, **12**, 63–72.
22 K. Kulangara and K. W. Leong, *Soft Matter*, 2009, **5**, 4072–4076.
23 ASTM-G31-72, American Society for Testing and Materials, Philadelphia, 2004.

